Applied Catalysis B: Environmental 187 (2016) 1–10

Contents lists available at ScienceDirect

Applied Catalysis B: Environmental

journal homepage: www.elsevier.com/locate/apcatb

Nitrogen and sulfur co-doped CNT-COOH as an efficient metal-free catalyst for the degradation of UV filter BP-4 based on sulfate radicals

Hui Liu[a,b], Ping Sun[b], Mingbao Feng[a], Hongxia Liu[a,b], Shaogui Yang[a], Liansheng Wang[a], Zunyao Wang[a,*]

[a] State Key Laboratory of Pollution Control and Resources Reuse, School of Environment, Nanjing University, Jiangsu, Nanjing 210023, PR China
[b] College of Biological and Chemical Engineering, Jiaxing University, Zhejiang, Jiaxing 314001, PR China

ARTICLE INFO

Article history:
Received 12 October 2015
Received in revised form
22 December 2015
Accepted 13 January 2016
Available online 16 January 2016

Keywords:
Carbon nanotube
Oxygenic functional groups
Nitrogen and sulfur doping
Sulfate radicals
Benzophenone-4

ABSTRACT

By using CNTs functionalized by oxygenic functional groups (—COOH or —OH) as the carbon source, novel catalysts of nitrogen (N) and sulfur (S) co-doped multi-walled carbon nanotubes (CNTs) were prepared for the first time by thermal decomposition. The obtained CNTs were characterized by SEM, TEM, BET, XPS, XRD, FT-IR and Raman spectroscopy. Additionally, the new material was used as a catalyst for the activation of peroxymonosulfate (PMS) for the degradation of benzophenone-4 (BP-4). Results indicated that the —COOH group plays an important role in the S doping process. Moreover, binary (N and S)-doped CNT-COOH (NS-CNT-COOH) exhibited a notably enhanced catalytic activity towards PMS for degrading BP-4. This activity level was approximately five-fold greater than that of singly (N)-doped CNT-COOH and binary (N and S)-doped CNT, and it even exceeded that of the metal catalyst $CuFe_2O_4$. The enhanced catalytic performance was attributed to the active sites generated by the introduced pyridinic and pyrrolic N atoms and thiophenic S atoms. The effects of various factors on the catalytic activity of NS-CNT-COOH were studied. Results revealed that the degradation efficiency of BP-4 increased with catalyst load, oxidant concentration and reaction temperature. In contrast, NS-CNT-COOH exhibited no remarkable catalytic activity towards peroxodisulfate (PDS) and H_2O_2. In the case of the NS-CNT-COOH/PMS system, a possible pathway for BP-4 degradation was proposed and based on detected intermediates. The mechanism was justified by theoretical calculations of the frontier electron densities, which have not been reported previously. Furthermore, mineralization, toxicity, stability and reusability tests suggested that the developed catalyst, NS-CNT-COOH, holds promise for practical application.

1. Introduction

The prospect of sulfate radicals ($SO_4^{\bullet-}$)-based advanced oxidation technologies (AOTs) being used in the field of wastewater treatment is good due to the strong oxidizing ability of these species [1–3]. Sulfate radicals, generated from either peroxymonosulfate (PMS) or peroxodisulfate (PDS), are more selective than hydroxyl radicals ($^{\bullet}OH$) for the oxidation of organic pollutants and could achieve better mineralization. They can be a promising alternative to $^{\bullet}OH$ for advanced oxidation in aqueous solutions [4,5]. The sulfate radical can be produced from the activation of PMS or PDS by various methods such as UV, heat, transition metals (Fe^{2+}, Co^{2}+, Cu^{2+}) or metal oxides (Fe_3O_4, CuO, $CuFe_2O_4$) [6–11]. However, the toxicity of the metal catalysts limited their practical applications due to the need of environmental protection.

Recent studies have demonstrated that nanostructured carbons, such as carbon nanotubes (CNTs) and graphene oxide, can be employed as green catalysts for the heterogeneous remediation of organic pollutants in water [12–17] and would completely avoid toxic metal leaching [18]. Importantly, the chemical doping of adventitious heteroatoms (N, S, B or P) into the carbon framework can remarkably enhance the catalytic activity of nanostructured carbons [19–27]. In particular, co-doping with two or three dopant elements of different electronegativities can result in a synergistic effect due to a unique electron distribution [28–30]. Although doped nanocarbons have been intensively investigated, the synthesis of N and S co-doped CNTs functionalized by oxygen-containing functional groups has rarely been reported.

Benzophenone-4 (BP-4) is one of the most common BP-type UV filters used in personal care products [31]. However, this compound has been detected in the environment [32] and may pose a

* Corresponding author.
E-mail address: wangzun315cn@163.com (Z. Wang).

http://dx.doi.org/10.1016/j.apcatb.2016.01.036
0926-3373/

serious public health hazard due to its potential endocrine disrupting effect [33]. As conventional processes in wastewater treatment plants (WWTPs) are unable to eliminate this emerging contaminant effectively, it is necessary and important to develop effective methods for the degradation and removal of BP-4 from the aqueous phase [34–37]. However, to date, the information about the $SO_4^{\bullet-}$ degradation process of BP-4 is limited, which hinders the application of this technique in BP-4 treatments. The key to $SO_4^{\bullet-}$ based AOTs is to develop highly efficient activation methods and catalysts for PDS and PMS. Thus, to develop highly active and environment-friendly catalysts for the activation of PDS and PMS is currently a hot research topic in the field of environmental catalysis.

Our previous study has found that a carboxylated carbon nanotube (CNT-COOH) catalyst can enhance the ozonation of indigo [17]. Therefore, we attempted to test the hypothesis of whether a co-doped CNT catalyst originating from CNTs functionalized by selective oxygenic functional groups can enhance the intrinsic reactivity and/or add new features to further promote catalysis. In this study, we chose CNTs functionalized by oxygenic functional groups as the carbon source and doped them with N and S for the first time. The characterization of this material was performed, and its performance as a metal-free catalyst for PMS activation was investigated. This study attempted to provide the basis for a new way to thoroughly treat the BP-4 wastewater with $SO_4^{\bullet-}$.

2. Experimental and theoretical methods

2.1. Chemicals and materials

BP-4 (CAS no: 4065-45-6, 98% purity) was obtained from J&K (Shanghai, China). Formic acid and methanol (for HPLC and LC–MS analysis) were of HPLC grade and obtained from Merck (Darmstadt, Germany). All of the other reagents were of analytical grade or higher. Ultrapure water (>18.2 MΩ cm) was prepared with a Milli-Q Plus system (Millipore, Bedford, USA). Functionalized CNTs were purchased from Chengdu Organic Chemicals Co. Ltd., Chinese Academy of Sciences (Chengdu, China). Their technical data are listed in Supporting information (Table S1).

2.2. Catalyst preparation

Doped CNTs were prepared by the thermal decomposition method. In this method, 1.0 g of CNTs was first finely milled with 1.0 g of thiourea and then transferred into a porcelain boat. The boat with the mixture was put into a tube furnace for calcination at 350 °C for 1 h at a heating rate of 10 °C/min under nitrogen flow and then cooled down to room temperature. The formed product was further crushed, washed by ethanol and ultrapure water and then dried overnight in a vacuum oven at 60 °C. Thus, N and S co-doped CNT samples were obtained.

The literature reported that graphitic-like nitrogen could be obtained at temperature over 600 °C [23], thus, other samples were synthesized at a high temperature. However, the samples calcined at 600 °C exhibited no remarkable enhancement in catalytic activity (Fig. S1), and the N-S co-doped CNT (NS-CNT-COOH) sample showed the highest activity; therefore, this material was chosen for detailed characterization and further oxidation reactions.

2.3. Characterization

Scanning electron microscopy (SEM) was performed with an S-3400 N II SEM (Hitachi, Japan). Transmission electron microscopy (TEM) image was obtained on a JEM-200CX TEM (JEOL, Japan). X-ray diffraction (XRD) was acquired by an X'TRA X-ray diffractometer (ARL, Switzerland). Fourier transform infrared (FT-IR) spectroscopy was recorded on a Nicolet-Nexus 470 FTIR spectrometer using KBr pellets (Thermo, USA). Raman spectra were recorded with a JY-HR800 spectrometer (Jobin Yvon, France). X-ray photoelectron spectroscopy (XPS) was obtained on a PHI 5000 VersaProbe system (UlVAC-PHI, Japan) using a monochromatic Al Kα X-ray source. Specific surface area (BET) and pore size distribution were measured at 77 K using an ASAP 2020 BET apparatus (Micromeritics, USA).

2.4. Catalytic oxidation procedure

The catalytic degradation tests were performed in 250 mL batch reactors at 25.0 ± 0.2 °C while being mixed at 200 rpm in a constant temperature water bath shaker. A specified amount of PMS and BP-4 solutions were introduced into the reactor. The solution pH was adjusted by H_2SO_4 and NaOH. Then the reaction was initiated by adding the catalyst. After a defined time interval, a sample was withdrawn, and immediately filtered through a 0.22 μm filter into an HPLC vial, which was pre- loaded with $NaNO_2$ or ascorbic acid to quench the reaction. Particularly, the potential effects of PMS dosage, catalyst dosage, and reaction temperature on the catalytic degradation of BP-4 were evaluated. All experiments were conducted in duplicate, and the mean values were reported.

2.5. Analytical methods

BP-4 was analyzed by an Agilent 1200 high performance liquid chromatography (HPLC) system equipped with a quaternary pump and a UV detector. A Zorbax 300SB-C18 column (4.6 × 150 mm, 5 μm) was used for the separation at 30 °C. The isocratic elution was 0.3% formic acid in water (50%) and methanol (50%) with a flow rate of 1 mL min^{-1}. The injection volume was 20 μL, and the detection wavelength was 286 nm.

For the identification of intermediate products, the aqueous phase was concentrated by an SPE workstation (Supleco, USA) using an Oasis HLB cartridge (Waters, USA). Mass spectrometry was performed by Agilent 1260 infinity high performance liquid chromatography system coupled with a high-resolution hybrid quadrupole time-of-flight mass spectrometer (LCMS-Triple TOF 5600, AB Sciex, Foster City, CA), which was equipped with an electrospray ionization (ESI) source operating in negative ion mode. The chromatographic separation was conducted at a total flow rate of 0.2 mL min^{-1} by a Thermo BDS Hypersil C18 column (100 × 2.1 mm, 2.4 μm). The mobile phase consisted of 0.3% formic acid in water (A) and methanol (B).

The total organic carbon (TOC) analysis was carried out on a Liqui TOCII analyzer (Elmentar, Germany). Based on the microplate toxicity analysis, the toxicities of the intermediate products against freshwater Photobacterium phosphoreum (*Q67*) were determined on an Infinite 200® PRO multimode microplate reader (Tecan Group Ltd., Switzerland) (Text S1). Three carboxylic acids (formate, acetate and oxalate) generated from the BP-4 oxidation were quantified by an ion-chromatograph system (ICS-1000, Dionex, USA) (Text S2).

2.6. Computational method

BP-4 was optimized at the B3LYP/6-311G** level using the Gaussian 03 software package [38], and the molecular orbital calculations were carried out using the optimized conformation. The integral equation formalism polarized continuum model (IEFPCM) within the self-consistent reaction field (SCRF) theory was used to consider the bulk solvent effect of water. The frontier electron densities (FEDs) of the highest occupied molecular orbital (HOMO) and the lowest unoccupied molecular orbital (LUMO) were obtained from the Gaussian output files. The values of $2FED^2_{HOMO}$ and $(FED^2_{HOMO} + FED^2_{LUMO})$ were calculated to predict the possi-

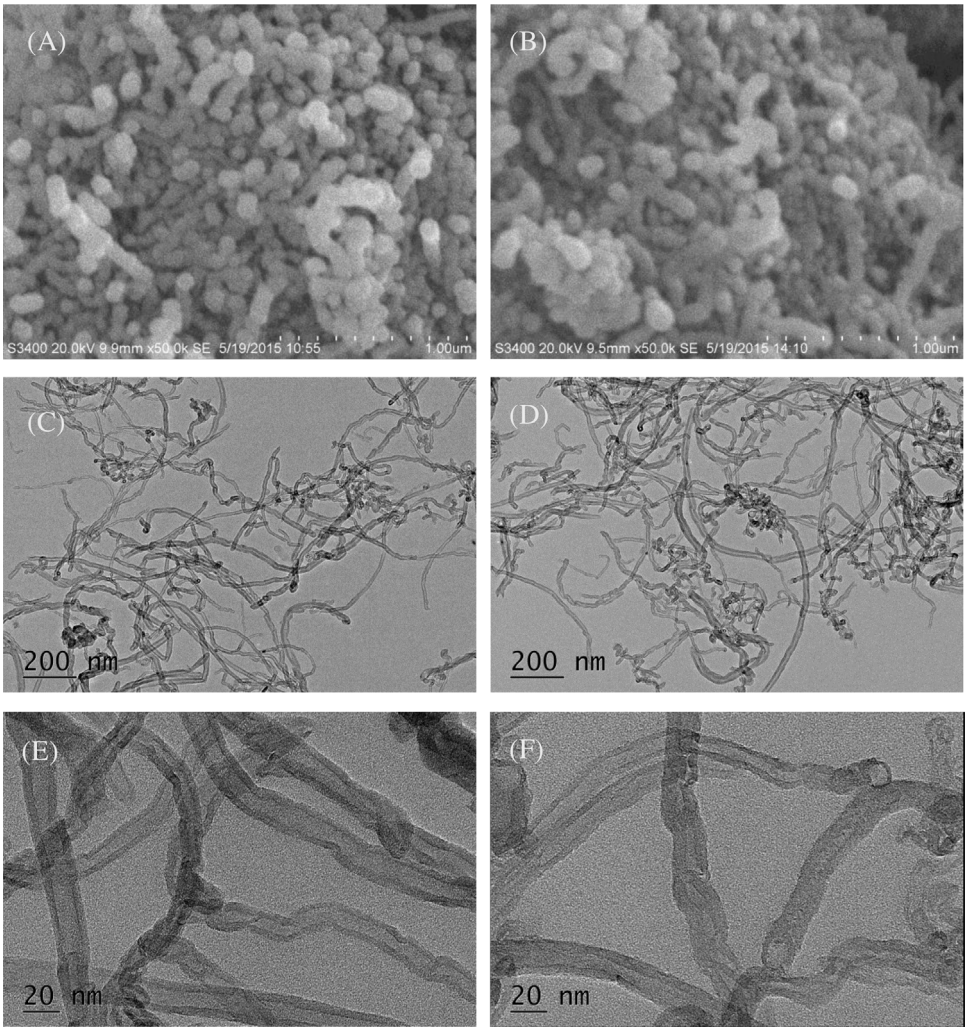

Fig. 1. SEM images of (A) CNT-COOH and (B) NS-CNT-COOH, TEM images of (C, E) CNT-COOH and (D, F) NS-CNT-COOH.

Table 1
Atomic composition of CNT and heteroatom- doped CNT samples (XPS).

Samples	C1s	O1s	N1s	S2p
CNT-COOH	94.63	5.37		
N-CNT-COOH(1)	97.16	1.58	1.27	
NS-CNT	96.83	1.44	1.56	0.17
NS-CNT-OH	93.00	1.98	4.82	0.20
NS-CNT-COOH	94.51	1.44	3.71	0.34
NS-CNT-COOH (used)	92.20	5.02	2.63	0.16

ble reaction sites for electron extraction and hydroxyl addition, respectively [39,40].

3. Results and discussion

3.1. The influences of different oxygen-containing functional groups

To investigate the influence of oxygen-containing functional groups on the doping process, different types of doped CNTs were prepared by carrying out the doping process on the CNTs with different oxygen-containing functional groups. Their elemental contents were determined by XPS analysis, as shown in Table 1. The oxygen content was reduced due to the decomposition of oxygen-containing functional groups. A single nitrogen doping level of 1.27% (N-CNT-COOH(1)) was achieved by thermally annealing CNT-COOHs with urea, which was higher than that of 0.88% obtained via CNTs with urea ammonium nitrate [26]. The nitrogen content of co-doped samples, NS-CNT, NS-CNT-OH and NS-CNT-COOH, were 1.56, 4.82 and 3.71%, respectively, with both doping and co-doping methods indicating that the oxygen-containing functional groups evidently promote the doping of nitrogen into CNTs. The sulfur content of NS-CNT, NS-CNT-OH and NS-CNT-COOH were 0.17, 0.20 and 0.34%, respectively, indicating that the oxygenic functional groups also evidently promote the sulfur doping of CNTs. This is because oxygen-containing functional groups on the CNT surface provided the additional active sites to react with N and S atoms. Recent studies have revealed that there is a gradual thermal transformation of nitrogen bonding configurations from the amide form of nitrogen to pyrrolic, then to pyridinic, and finally to "graphitic" nitrogen in graphene sheets upon increasing the annealing temperature [23,24]. Similarly, in this study NH_3, CS_2 and HNCS (produced by decomposition of thiourea) might first be connected to oxygen-containing functional groups at CNT edges or defect sites at a relatively low temperature, and then these intermediates were transformed to pyridinic and pyrrolic N and thiophenic S.

The S content was relatively low maybe because the atomic radius of S (1.03 Å) is larger than those of N (0.71 Å) and C (0.75 Å), which makes it more difficult to be incorporated into the CNT [30]. Moreover, sulfur doping usually occurs in only one binding configuration (i.e. thiophenic S), thus, the doping levels of sulfur were lower compared with those of nitrogen [29]. Meanwhile, the lower S con-

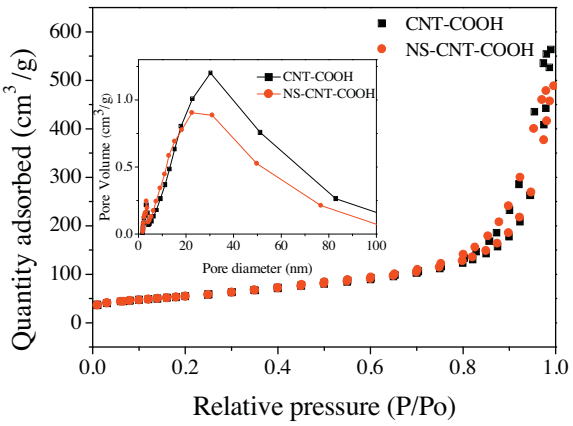

Fig. 2. Nitrogen adsorption-desorption isotherms of CNT-COOH and NS-CNT-COOH and corresponding pore – size distribution plots calculated by BJH method from desorption branch isotherms.

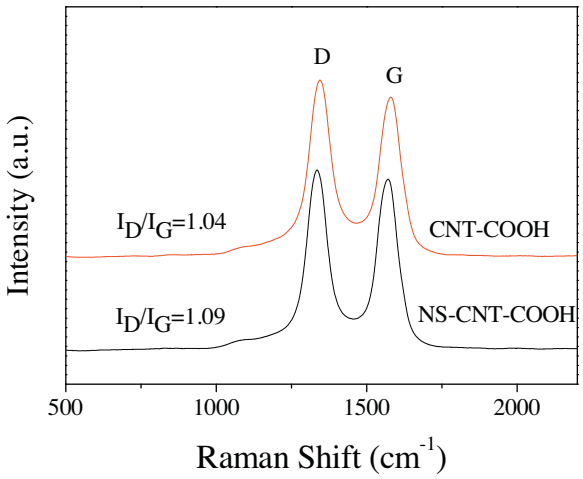

Fig. 3. Raman spectra for CNT-COOH and NS-CNT-COOH.

tent might also be explained by the fact that thiourea prossesses an atomic composition of N that is twice the atomic composition of S. It is noteworthy that the S doping level of NS-CNT-COOH is higher than that of the others, which showed the functional —COOH group plays a unique role in the S doping process. The nitrogen concentration of NS-CNT-COOH (3.71%) is higher than that of N-CNT-COOH (1.27%), which may imply a synergistic interaction between N and S in the co-doped sample that dramatically increased the N content.

3.2. Characterization of catalysts

The morphologies and structures of CNT-COOH and the N-S co-doped CNT sample (NS-CNT-COOH) were obtained from SEM and TEM images (Fig. 1). Both samples exhibit significant aggregation (Fig. 1A and B). Fig. 1C-F shows the TEM images for CNT-COOH and NS-CNT-COOH. These images further confirmed that the nitrogen and sulfur doping did not break the tubular structure of the CNTs.

Nitrogen adsorption–desorption isotherms and pore size distribution curves of bare and doped CNT samples are shown in Fig. 2 and displayed type II isotherms. The wide hysteresis area in the nitrogen adsorption–desorption isotherms can clearly be seen in the cases of CNT-COOH and NS-CNT-COOH, suggesting the wide distribution of pores in both samples. The mesopore diameter did not show much change after the introductions of heteroatoms. The specific surface areas (SSAs) of CNT-COOH and NS-CNT-COOH were both 192.2 $m^2\,g^{-1}$. The SSA of NS-CNT-COOH has no significant change after doping with N and S atoms. Mesopores centred at approximately 30 nm were observed for both samples, indicating no significant change in the porous structure by the co-doping of sulfur and nitrogen.

To further evaluate the structural defects induced by heteroatom doping in CNTs, Raman analysis was carried out on pristine and doped CNT samples, as shown in Fig. 3. Two distinct peaks appear at approximately 1340 and 1570 cm^{-1}, corresponding to the D and G band, respectively. Generally, the I_D/I_G value is known to be proportional to the degree of disorder in carbon. A higher I_D/I_G value indicates a higher disorder, whereas a lower value signifies less disorder in the graphitic plane [19]. The I_D/I_G value was 1.09 for NS-CNT-COOH, which was higher than the value of 1.04 for CNT-COOH. This reveals that the defects were introduced in the carbon network by co-doping with N with S, and the extent of the carbon disorder in NS-CNT-COOH was higher than that in CNT-COOH.

To investigate the chemical composition and dopant of NS- CNT-COOH, XPS analysis was carried out, as shown in Fig. 4. Apparently, C, O, N and S peaks can be seen in Fig. 4A. In NS- CNT-COOH, nitrogen is doped in the carbon lattice as pyridinic (N1, 398.7 eV) and pyrrolic N (N2, 400.1 eV) (Fig. 4B), whereas quaternary N (401.8 eV) and oxides of nitrogen (402.4 eV) were not found. Sulfur dopants were structurally bound mainly in the form of thiophenic S (S1, C–S–C, 164.1 and 165.4 eV), while others were in the form of oxidized S (S2, C–SO*x* — C, 168.5 and 169.7 eV) (Fig. 4C). The formation of pyridinic N, pyrrolic N and thiophenic S indicated that N and S atoms were successfully doped into the carbon framework.

Fig. S2 shows the XRD patterns for CNT-COOH and NS-CNT-COOH. Typical diffraction peak for (002) at 26°, (100) at 43° and (004) at 54° can be seen in both samples. In addition, there were no obvious shifting of these diffraction peaks after nitrogen and sulfur doping, indicating that there was no obvious change in the crystal structure of the catalyst during the doping process. Fig. S3 shows the FT-IR spectra of CNT-COOH and NS- CNT-COOH. The peak at approximately 3400 cm^{-1} was assigned to the stretching vibration of hydroxyl groups of adsorbed water, and the peak at 1630 cm^{-1} corresponded to the valence oscillations of C=C in the benzene ring. No obvious peak characteristic of —COOH at 1720 cm^{-1} was observed, possibly owing to the low —COOH content of CNT–COOH (1.23 wt%, determined by XPS and the Boehm titration method).

3.3. Catalytic oxidation of BP-4

To evaluate the catalytic oxidation efficiencies of BP-4 on various CNT catalysts, a set of experiments was conducted under different experimental conditions. As shown in Fig. 5, BP-4 was rapidly degraded by PMS/NS-CNT-COOH and BP-4 was completely eliminated within 30 min using 1.000 g L^{-1} PMS and 0.100 g L^{-1} NS-CNT-COOH. Meanwhile, PMS alone led to the removal of 8% BP-4 in 1 h, whereas NS-CNT-COOH alone removed very little BP-4 (5%). Additionally, CNT-COOH was more efficient than the pristine CNT sample. Under the tested conditions, the BP-4 degradation approximately followed pseudo-first-order kinetics. After doping, the apparent reaction rate constant (k) of NS-CNT-COOH was 0.1617 min^{-1}, which was 28.9, 26.8, 5.5, 5.1, 5.6 and 4.6 times higher than that of CNT, CNT-OH, CNT-COOH, NS-CNT, NS-CNT-OH and N-CNT-COOH. Thus, it can be deduced that sulfur can serve as a promising co-dopant to further improve the catalytic activity of chemically modified CNTs towards PMS, because co-doped CNT-COOH (NS-CNT-COOH) exhibited a notably enhanced catalytic activation of PMS for BP-4 degradation when compared with that of singly N-doped CNT-COOH.

Additionally, the impacts of several parameters, such as catalyst load, PMS dose and temperature, were also evaluated and are shown in Fig. 6. The influence of catalyst loading on the CNT-

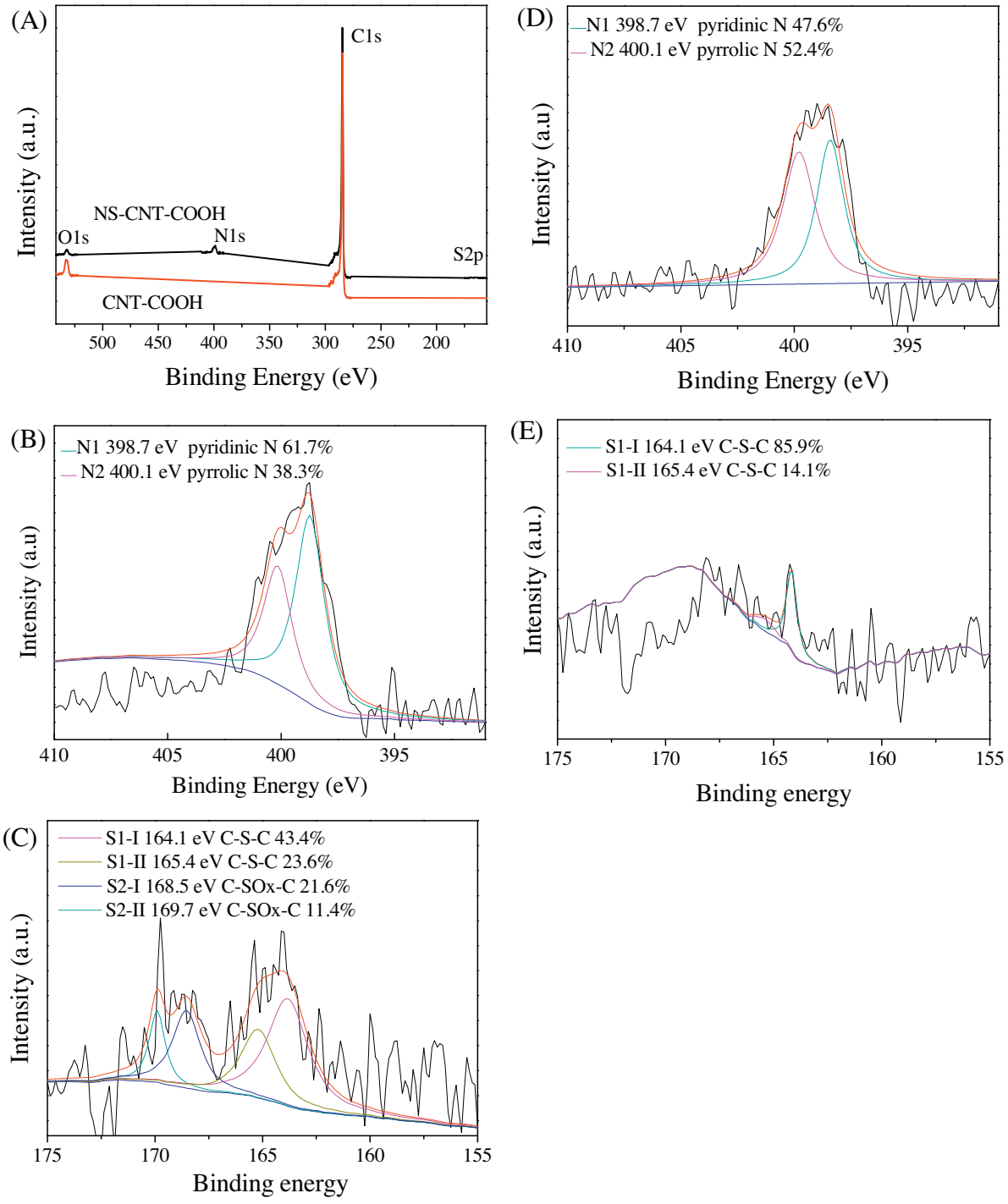

Fig. 4. (A) XPS survey spectra of CNT-COOH and NS-CNT-COOH, (B) N1s and (C) S2p spectrum of fresh NS-CNT-COOH, and (D) N1s and (E) S2p spectrum of used NS-CNT-COOH.

catalyzed BP-4 degradation was investigated with different catalyst doses (0.025, 0.050, 0.100 and 0.200 g L^{-1}). As shown in Fig. 6A, the degradation efficiency of BP-4 increased with NS-CNT-COOH loading. This suggests that a higher catalyst loading would provide more active sites for the formation of $SO_4^{\bullet-}$ and that the degradation rate was increased.

The BP-4 degradation efficiency was also affected by the PMS dose. As shown in Fig. 6B, the degradation efficiency was 58% at 10 min with 0.250 g L^{-1} PMS, and further increased to 95% with 2.000 g L^{-1} PMS. In addition to the radical-scavenging ability of PMS being increased with the PMS dose, the removal efficiency was also progressively enhanced, indicating that the active sites on the NS-CNT-COOH surface were still not completely occupied by PMS even at the concentration of 2.000 g L^{-1} with a NS-CNT-COOH dose of 0.100 g L^{-1}. However, compared with the metal-based catalyst, NS-CNT-COOH exhibited a greater potential to catalytic activate a high PMS dose for BP-4 degradation.

The degradation reaction of BP-4 was also significantly influenced by the reaction temperature. As shown in Fig. 6C, the higher the temperature, the faster the BP-4 degradation. The degradation rate constants (k) were 0.1629, 0.2844 and 0.5277 min^{-1} at 25, 35 and 45 °C. In addition, by using the Arrhenius equation with the experimental data, the activation energy (*Ea*) of NS-CNT-COOH for the catalyzed BP-4 oxidative degradation was estimated to be

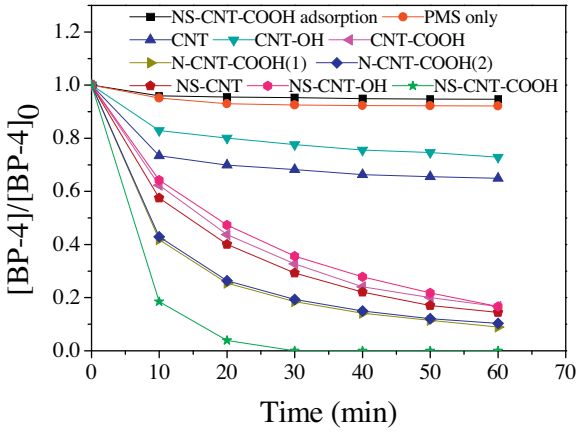

Fig. 5. BP-4 removal efficiencies on various carbon catalysts. Condition: [BP-4] = 0.010 g L^{-1}, initial pH 7.0 ± 0.2, [catalyst] = 0.100 g L^{-1}, [PMS] = 1.000 g L^{-1}, T = 25 °C.

46.3 kJ mol^{-1} (R^2 = 0.9976). It can be deduced that higher temperatures were conducive to the removal rate.

3.4. Oxidation intermediates and pathways

Oxidation intermediates of the BP-4 catalytic PMS degradation were identified by LC-TOF-MS in the negative mode with MS^2 Scan. Seven products were observed; their MS data and proposed structures are shown in Table S2 and Fig. S4. In most cases, there was good agreement (< 3 ppm error) between the accurate mass measurements and the proposed molecular formulas, providing a high degree of certainty in the structural assignments. In this sense, it is possible to propose the molecular structures of the identified intermediates from some information of the BP-4 molecule and the PMS oxidation mechanism.

Based on the chemical structures of the identified oxidation intermediates and earlier findings on the oxidation of aromatic compounds, as well as details on the BP-4 degradation in other reaction systems, possible transformation pathways of BP-4 were tentatively proposed (Fig. 7). Firstly, the C—H bond at C(4) in the BP-4 molecule was attacked by •OH to form the hydroxylated BP-4 (P1), and sequential hydroxylation of the aromatic ring of P1 can generate P2. The latter underwent further oxidation to produce P3 and subsequently the oxidation product P7. On the other hand, when the C(5)-C(8) bond was broken, P4 was generated and further oxidized to P5. Additionally, a demethylation of the methoxy moiety of BP-4 forms P6.

To further rationalize the proposed reaction mechanisms and products, the frontier electron densities of the BP-4 anion were calculated and the results are listed in Table 2. Generally, in an electrophilic reaction electrons can be easily extracted from atoms with higher values of $2FED^2_{HOMO}$, while the addition of radicals usually takes place at positions with higher $FED^2_{HOMO} + FED^2_{LUMO}$ values. As shown in Table 2, the C(7) and C(4) atoms of the BP-4 anion were found to possess the higher $FED^2_{HOMO} + FED^2_{LUMO}$ values, which indicated that they are the most reasonable sites for the addition of a hydroxyl radical. Thus, the formation of the hydroxylated intermediates P1, P4 and P6 (Fig. 7) can be attributed to the attack of hydroxyl radicals. In addition, the C(5) atom was found to possess the highest $2FED^2_{HOMO}$ value. Therefore, this position was a likely location for $SO_4^{\bullet -}$ attack and electron extraction, leading to the opening of a five-membered heterocyclic ring and generating intermediate P7.

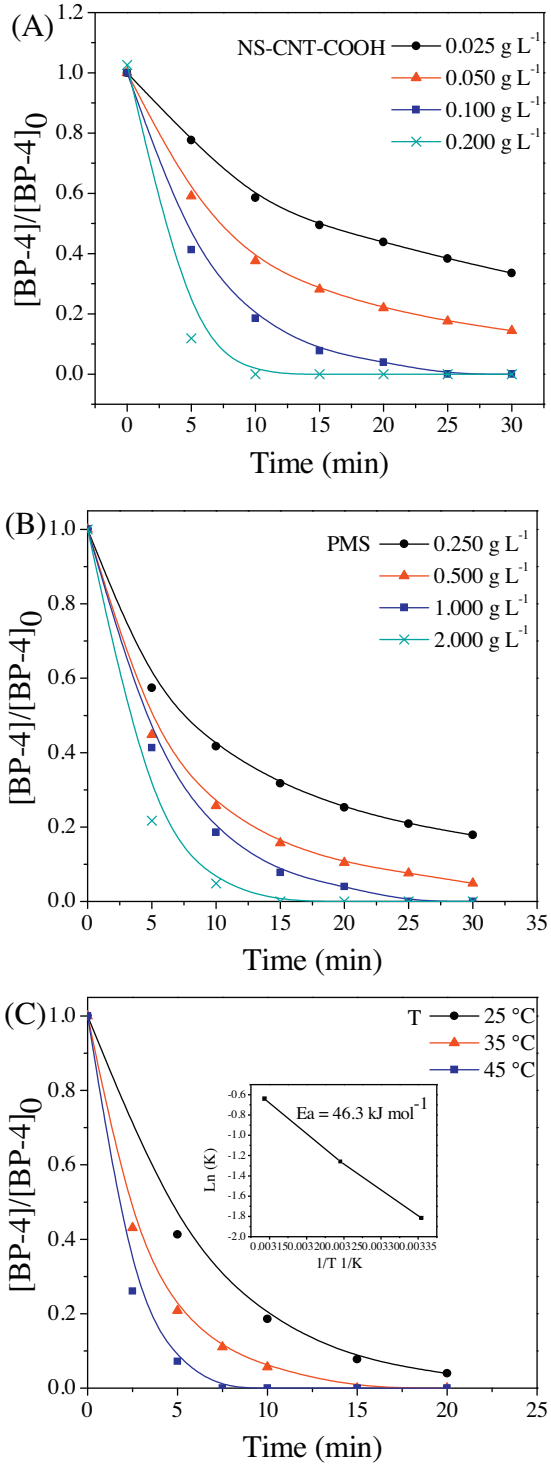

Fig. 6. Influences of (A) NS-CNT-COOH dose, (B) PMS dose, and (C) reaction temperature. Condition: [BP-4] = 0.010 g L^{-1}, initial pH 7.0 ± 0.2, [NS-CNT-COOH] = 0.100 g L^{-1}, PMS = 1.000 g L^{-1}, T = 25 °C.

3.5. Activation mechanisms of PMS with NS-CNT-COOH

The activation processes of PMS on NS-CNT-COOH are summarized in Scheme 1. In this study, the activity of CNT-COOH was mainly attributed to sp^2 carbon and the —COOH group. For NS-CNT-COOH, the sp^2 carbon and functional group still worked as active sites. The significant improvement in the catalytic activity of NS-CNT-COOH for PMS activation was then attributed to the

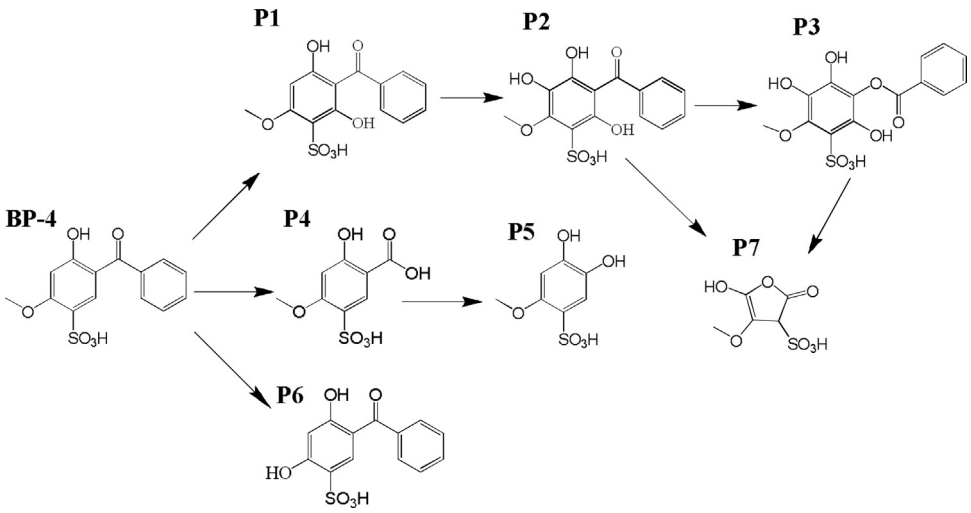

Fig. 7. Proposed reaction pathways for the BP-4 oxidation by PMS.

Table 2
Frontier electron densities on atoms of BP-4 calculated at the B3LYP/6-311G** level by Gaussian 03 program.

Atom	$2FED^2_{HOMO}$	$FED^2_{HOMO}+FED^2_{LUMO}$	Atom	$2FED^2_{HOMO}$	$FED^2_{HOMO}+FED^2_{LUMO}$
C(1)	0.000616	0.008068	C(8)	0.000784	0.058117
C(2)	0.004606	0.072190	C(9)	0.001927	0.063168
C(3)	0.015286	0.029638	C(10)	0.001393	0.027700
C(4)	0.005024	**0.083975**	C(11)	0.000505	0.073554
C(5)	**0.022474**	0.036648	C(12)	0.000286	0.004909
C(6)	0.005384	0.054583	C(13)	0.000155	0.062973
C(7)	0.001312	**0.169717**			

Numbers in bold means the higher $2FED^2_{HOMO}$ or $FED^2_{HOMO}+FED^2_{LUMO}$ values.

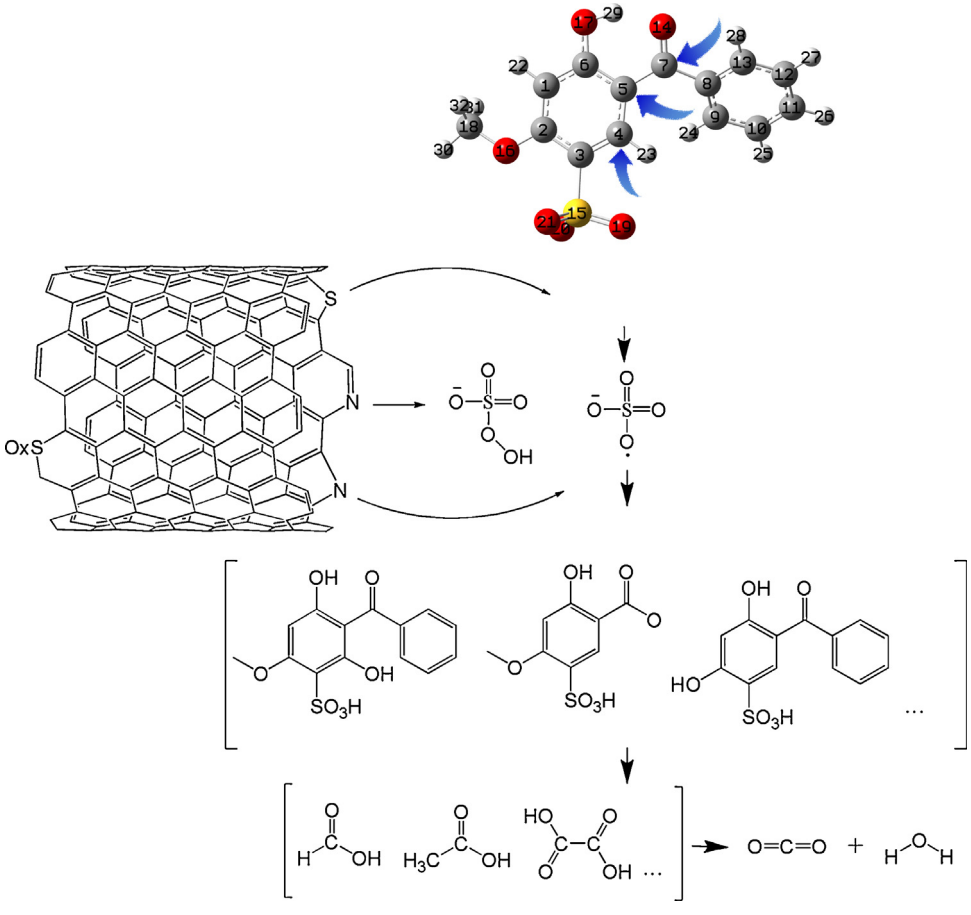

Scheme 1. Nitrogen and sulfur co-doped CNT-COOH in activation of PMS for BP-4 oxidation.

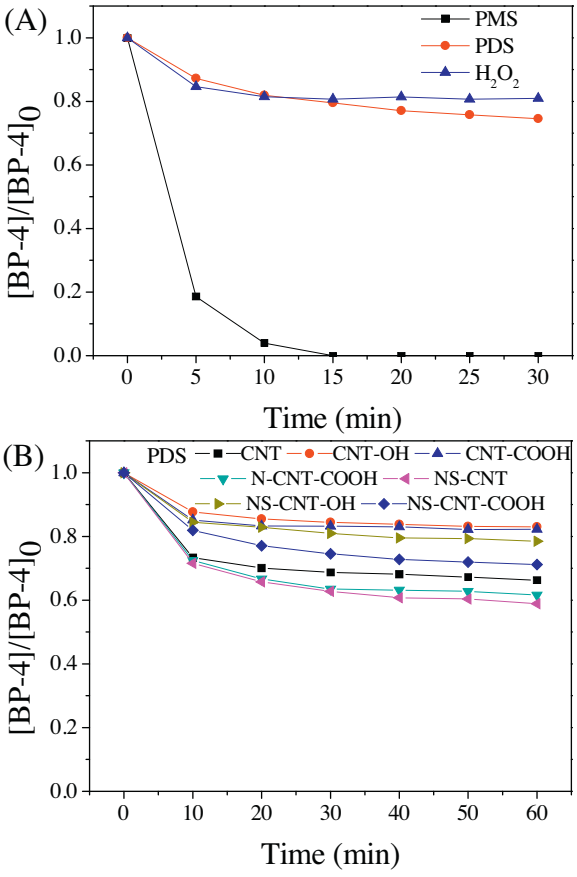

Fig. 8. BP-4 degradation (A) on NS-CNT-COOH with various oxidants, and (B) on various carbon catalysts with PDS. Condition: [BP-4] = 0.010 g L^{-1}, initial pH 7.0 ± 0.2, [catalyst] = 0.100 g L^{-1}, [oxidant] = 3.25 mM, T = 25 °C.

introduced pyridinic and pyrrolic N atoms and thiophenic S atoms. First, the doped nitrogen has a higher electronegativity (3.04) than carbon (2.55), while sulfur exhibits a closely matched electronegativity (2.58). These dopants would disrupt the chemically inert nature of the carbon network, thus, inducing larger spin and charge densities on the neighboring carbons. As a consequence, positively charged neighboring carbons can be created, which might serve as the active sites to facilitate the adsorption of HSO_5^- and to break the O—O bond ($HO–SO_4^-$) for PMS activation [41]. Second, the C—C bond length of sp^2-hybridized carbon changes from 147 to 210 pm with the introduction of either N or S [29]. Finally, there may be a synergistic effect resulting from the N–S co-doping of CNTs, which can also redistribute the spin and charge densities, activate the sp^2 hybridized carbon and promote the electron transfer [28]. In conclusion, the changes in electronegativity and in bond length of the carbon framework, as well as the synergistic effects due to N–S co-doping, can make the carbon surface asymmetric in nature and present greater catalytic activity towards PMS.

3.6. Comparison of peroxides and reported catalysts

The decontamination efficiencies of PDS/NS-CNT-COOH and H_2O_2/NS-CNT-COOH were investigated and compared with that of PMS/NS-CNT-COOH. However, PDS/NS-CNT-COOH and H_2O_2/NS-CNT-COOH showed almost no degradation of BP-4 (Fig. 8A). PDS activation seems to be different from PMS. As shown in Fig. 8B, the activity of CNT-OH and CNT-COOH towards PDS were lower than that of the pristine CNT, suggesting that oxygen-containing functional groups were not effective for PDS activation. Moreover, the addition of N and S dopants to functionalized CNTs was also ineffective in activating PDS; however, the activity of NS-CNT towards PDS was increased over that of the pristine species. These results suggested that PMS can be easily activated by the heterogeneous catalytic oxidation due to its asymmetric structure.

A recent study demonstrated that N-CNT can effectively activate PMS to degrade phenol. Thus, the singly nitrogen doped CNT-COOH was prepared by the above method consisting of the addition of urea (N-CNT-COOH (1)). Meanwhile, according to a previous doping method [27], surface nitrogen modification was conducted by annealing CNT-COOH (instead of CNT) with ammonium nitrate, obtaining N-CNT-COOH (2). Moreover, Ding et al. and Guan et al. have found that porous copper ferrite ($CuFe_2O_4$) exhibits a remarkable catalytic activity towards PMS [8,9], and Leng et al. have reported that polyhydroquinone-coated Fe_3O_4 (PHQ/Fe_3O_4) shows better catalytic performance than PHQ and Fe_3O_4 [42]; thus, $CuFe_2O_4$ nanoparticles were prepared by the sol-gel combustion method described in [9], and polyhydroquinone/$CuFe_2O_4$ (PHQ/$CuFe_2O_4$) was synthesized according to the oxidative polymerization of 1,4-hydroquinone [42]. The catalytic activities of singly N-doped CNTs (Fig. 4) and metal oxides ($CuFe_2O_4$ and PHQ/$CuFe_2O_4$, Fig. S5) were also evaluated. The results showed that the NS-CNT-COOH/PMS system has a superior efficiency for the degradation of BP-4.

3.7. The mineralization and toxicity changes

During the BP-4 oxidation process, the TOC removal was measured to reflect the mineralization of BP-4 (Fig. S6). The results indicated that TOC reduction proceeded much more slowly than did the degradation of BP-4. After 30 min, BP-4 was completely decomposed, but the TOC removal was approximately 20%. It was likely that some recalcitrant products were produced during the oxidation, such as small molecular carbolic acids, etc. The decrease in pH value from 7.00 to 3.23 (Fig. S7) might indicate the formation of small-molecular carbolic acids. Moreover, an abundance of oxalate generated by the BP-4 oxidation were detected by the ion-chromatograph system (Fig. S8), whereas formate and acetate were not detected because of their instabilities. Finally, the degradation of BP-4 was concluded by mineralization to CO_2 and H_2O [9,26]. The mineralization pathway is shown in Scheme 1.

Because BP-4 oxidation can possibly generate intermediates that are more toxic than the parent compound, it is necessary to measure the changes in toxicity during the oxidative process of BP-4. In this study, toxicity tests were performed using freshwater Photobacterium phosphoreum (Vibrio qinghaiensis sp Q67) (Fig. S9). After treatment, the relative toxicity of the transformation products began to increase and was highest after 10 min, which indicated the presence of intermediate products with higher toxicities. With an extended period of time (20 min) and further oxidation of the intermediate products, the toxicity can be eliminated. On the whole, the treated solution showed no obvious toxicity to Q67. Meanwhile, acute aquatic toxicities (LC_{50}) of BP-4 and its degradation products were predicted by the Consensus method using the Toxicity Estimation Software Tool (T.E.S.T., version 4.1) [43] (Table S3) and classified according to the Globally Harmonized System of Classification and Labelling of Chemicals (GHS) [44] (Table S4). As seen in Table S3, all of the intermediates except P1 were less toxic than the parent compound. Especially, the final intermediates (P4, P5 and P7) were not at all harmful (>100 mg/L) to fish.

3.8. Stability and reusability of NS-CNT-COOH

To assess the potential of the developed catalyst for further practical application, the used catalyst was collected from the reaction solution by vacuum filtration, then washed by ultrapure water, and dried in a vacuum oven at 60 °C for 8 h. As shown in Fig. 9, the

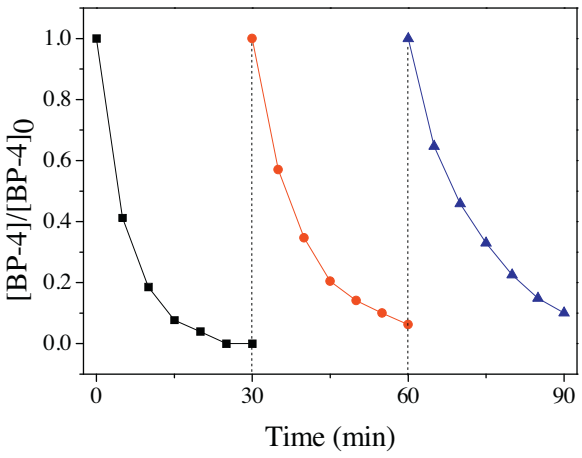

Fig. 9. Degradation kinetics of BP-4 using the recycled catalysts. Condition: [BP-4] = 0.010 g L^{-1}, initial pH 7.0 ± 0.2, [NS-CNT-COOH] = 0.100 g L^{-1}, PMS = 1.000 g L^{-1}, T = 25 °C.

degradation rates of the recycled catalysts were similar to that of the fresh one, which indicated that NS-CNT-COOH is stable in the present study.

Meanwhile, the used NS-CNT-COOH was characterized by XRD, TEM and XPS. The XRD patterns (Fig. S2) and TEM images (Fig. S10) shows that NS-CNT-COOH remained the tubular and crystal structures very well after being used. XPS survey shows that the O content increased to 5.02%, whereas the N and S content of NS-CNT-COOH decreased (Table 1). Furthermore, the content ratio of pyridinic N to pyrrolic N decreased from 1.61 to 0.91, and the peaks of oxidized S (S2, C–SO*x* — C, 168.5 and 169.7 eV) disappeared, as seen in Fig. 4D-E. Oxidized S is considered to be inactive [29], thus, the primary reason for the reduced of degradation efficiency may be the loss of pyridinic N, which leads to less catalytic activity. Overall, the developed novel catalyst NS-CNT-COOH holds promise for practical applications.

4. Conclusions

Employing CNT-COOH as a carbon source, an N–S co-doped CNT sample was synthesized and characterized. Then, its performance in the metal-free activation of PMS for the catalytic oxidation of BP-4 was investigated. The experimental results indicated that different oxygenic groups on the CNT surface demonstrated influenced the doping process differently. N and S dopants were significantly more active towards PMS than the oxygen-containing groups, while the dopants were not effective for PDS activation. The degradation was found to follow pseudo-first order kinetics, and the degradation rate increased with the catalyst loading, PMS dosage, and reaction temperature. Seven intermediate oxidative products were detected, and their decomposition pathways were proposed and well confirmed by theoretical calculations of frontier electron densities. Furthermore, NS-CNT-COOH holds promise for practical application due to its good stability and reusability. This work may facilitate the development and application of novel doped CNT-based materials with functionalized surfaces.

Acknowledgments

This research was financially supported by the National Natural Science Foundation of China (Nos. 21377051, 21407061 and 21577063), the Major Science and Technology Program for Water Pollution Control and Treatment of China (No. 2012ZX07506-001), the Scientific Research Foundation of Graduate School of Nanjing University (2013CL08) and the Planned Science and Technology Project of Jiaxing (2014AY21013).

Appendix A. Supplementary data

Supplementary data associated with this article can be found, in the online version, at http://dx.doi.org/10.1016/j.apcatb.2016.01.036.

References

[1] X.X. He, A.A. de la Cruz, K.E. O'Shea, D.D. Dionysiou, Kinetics and mechanisms of cylindrospermopsin destruction by sulfate radical-based advanced oxidation processes, Water Res. 63 (2014) 168–178.
[2] Y. Yang, J.J. Pignatello, J. Ma, W.A. Mitch, Comparison of halide impacts on the efficiency of contaminant degradation by sulfate and hydroxyl radical-based advanced oxidation processes (AOPs), Environ. Sci. Technol. 48 (2014) 2344–2351.
[3] M. Ahmad, A.L. Teel, R.J. Watts, Mechanism of persulfate activation by phenols, Environ. Sci. Technol. 47 (2013) 5864–5871.
[4] T. Zhang, Y. Chen, Y.R. Wang, J. Le Roux, Y. Yang, J.P. Croueí, Efficient peroxydisulfate activation process not relying on sulfate radical generation for water pollutant degradation, Environ. Sci. Technol. 48 (2014) 5868–5875.
[5] S.H. Yuan, P. Liao, A.N. Alshawabkeh, Electrolytic manipulation of persulfate reactivity by iron electrodes for trichloroethylene degradation in groundwater, Environ. Sci. Technol. 48 (2014) 656–663.
[6] H.Z. Liu, T.A. Bruton, F.M. Doyle, D.L. Sedlak, In situ chemical oxidation of contaminated groundwater by persulfate: decomposition by Fe(III)- and Mn(IV)- containing oxides and aquifer materials, Environ. Sci. Technol. 48 (2014) 10330–10336.
[7] X.M. Xiong, B. Sun, J. Zhang, N.Y. Gao, J.M. Shen, J.L. Li, X.H. Guan, Activating persulfate by Fe^0 coupling with weak magnetic field: performance and mechanism, Water Res. 62 (2014) 53–62.
[8] Y.H. Guan, J. Ma, Y.M. Ren, Y.L. Liu, J.Y. Xiao, L.Q. Lin, C. Zhang, Efficient degradation of atrazine by magnetic porous copper ferrite catalyzed peroxymonosulfate oxidation via the formation of hydroxyl and sulfate radicals, Water Res. 47 (2013) 5431–5438.
[9] Y.B. Ding, L.H. Zhu, N. Wang, H.Q. Tang, Sulfate radicals induced degradation of tetrabromobisphenol A with nanoscaled magnetic $CuFe_2O_4$ as a heterogeneous catalyst of peroxymonosulfate, Appl. Catal. B: Environ. 129 (2013) 153–162.
[10] Y.X. Wang, H.Q. Sun, H.M. Ang, M.O. Tadé, S.B. Wang, Magnetic Fe_3O_4/carbon sphere/cobalt composites for catalytic oxidation of phenol solutions with sulfate radicals, Chem. Eng. J. 245 (2014) 1–9.
[11] P.H. Shi, R.J. Su, F.Z. Wan, M.C. Zhu, D.X. Li, S.H. Xu, Co_3O_4 nanocrystals on graphene oxide as a synergistic catalyst for degradation of orange II in water by advanced oxidation technology based on sulfate radicals, Appl. Catal. B: Environ. 123–124 (2012) 265–272.
[12] H. Lee, H.J. Lee, J. Jeong, J. Lee, N.B. Park, C. Lee, Activation of persulfates by carbon nanotubes: oxidation of organic compounds by nonradical mechanism, Chem. Eng. J. 266 (2015) 28–33.
[13] A. Goncalves, J.J. Orfao, M.F.R. Pereira, Ozonation of bezafibrate promoted by carbon materials, Appl. Catal. B: Environ. 140 (2013) 82–91.
[14] A.G. Goncalves, J.L. Figueiredo, J.J. Orfao, M.F. Pereira, Influence of the surface chemistry of multi-walled carbon nanotubes on their activity as ozonation catalysts, Carbon 48 (2010) 4369–4381.
[15] A.G. Goncalves, J.J. Orfao, M.F.R. Pereira, Catalytic ozonation of sulphamethoxazole in the presence of carbon materials: catalytic performance and reaction pathways, J. Hazard. Mater. 239 (2012) 167–174.
[16] A.G. Goncalves, J.J. Orfao, M.F.R. Pereira, Ozonation of erythromycin over carbon materials and ceria dispersed on carbon materials, Chem. Eng. J. 250 (2014) 366–376.
[17] R.J. Qu, B.Z. Xu, L.J. Meng, L.L. Wang, Z.Y. Wang, Ozonation of indigo enhanced by carboxylated carbon nanotubes: performance optimization, degradation products, reaction mechanism and toxicity evaluation, Water Res. 68 (2015) 316–327.
[18] H.Q. Sun, Y.X. Wang, S.Z. Liu, L. Ge, L. Wang, Z.H. Zhu, S.B. Wang, Facile synthesis of nitrogen doped reduced grapheme oxide as a superior metal-free catalyst for oxidation, Chem. Commun. 49 (2013) 9914–9916.
[19] D. Liu, X.P. Zhang, T.Y. You, Urea-treated carbon nanofibers as efficient catalytic materials for oxygen reduction reaction, J. Power Sources 273 (2015) 810–815.
[20] Z. Yang, Z. Yao, G.F. Li, G.Y. Fang, H.G. Nie, Z. Liu, X.M. Zhou, X.A. Chen, S.M. Huang, Sulfur-doped graphene as an efficient metal-free cathode catalyst for oxygen reduction, ACS Nano 6 (2012) 205–211.
[21] X.A. Chen, X.H. Chen, X. Xu, Z. Yang, Z. Liu, L.J. Zhang, X.J. Xu, Y. Chen, S.M. Huang, Sulfur-doped porous reduced graphene oxide hollow nanosphere frameworks as metal-free electrocatalysts for oxygen reduction reaction and as supercapacitor electrode materials, Nanoscale 6 (2014) 13740–13747.
[22] Y.M. Lin, D.S. Su, Fabrication of nitrogen-modified annealed nanodiamond with improved catalytic activity, ACS Nano 8 (2014) 7823–7833.

[23] J. Wu, C. Jin, Z.R. Yang, J.H. Tian, R.Z. Yang, Synthesis of phosphorus-doped carbon hollow spheres as efficient metal-free electrocatalysts for oxygen reduction, Carbon 82 (2015) 562–571.
[24] Y. Chen, B.Q. Xie, Y.T. Ren, M.Y. Yu, Y. Qu, T. Xie, Y. Zhang, Y.C. Wu, Designed nitrogen doping of few-layer grapheme functionalized by selective oxygenic groups, Nanoscale Res. Lett. 9 (2014) 646.
[25] Z.G. Mou, X.Y. Chen, Y.K. Du, X.M. Wang, P. Yang, S.D. Wang, Forming mechanism of nitrogen doped graphene prepared by thermal solid-state reaction of graphite oxide and urea, Appl. Surf. Sci. 258 (2011) 1704–1710.
[26] H.Q. Sun, C. Kwan, A. Suvorova, H.M. Ang, M.O. Tadé, S.B. Wang, Catalytic oxidation of organic pollutants on pristine and surface nitrogen-modified carbon nanotubes with sulfate radicals, Appl. Catal. B: Environ. 154–155 (2014) 134–141.
[27] J.X. Xu, L.H. Guan, Toward understanding the active site for oxygen reduction reaction on phosphorus-encapsulated single walled carbon nanotubes, RSC Adv. 3 (2013) 5577–5582.
[28] J. Restivo, R.P. Rocha, A.M.T. Silva, J.J.M. Órfão, M.F.R. Pereira, J.L. Figueiredo, Catalytic performance of heteroatom–modified carbon nanotubes in advanced oxidation processes, Chin. J. Catal. 35 (2014) 896–905.
[29] F. Razmjooei, K.P. Singh, M.Y. Song, J.S. Yu, Enhanced electrocatalytic activity due to additional phosphorous doping in nitrogen and sulfur-doped graphene: a comprehensive study, Carbon 78 (2014) 257–267.
[30] X.G. Duan, K. O'Donnell, H.Q. Sun, Y.X. Wang, S.B. Wang, Sulfur and nitrogen Co-doped graphene for metal-free catalytic oxidation reactions, Small 11 (2015) 3036–3044.
[31] M. Xiao, D.B. Wei, J.X. Yin, G.H. Wei, Y.G. Du, Transformation mechanism of benzophenone-4 in free chlorine promoted chlorination disinfection, Water Res. 47 (2013) 6223–6233.
[32] P. Gago-Ferrero, N. Mastroianni, M.S. Diaz-Cruz, D. Barcelo, Fully automated determination of nine ultraviolet filters and transformation products in natural waters and wastewaters by on-line solid phase extraction-liquid chromatography-tandem mass spectrometry, J. Chromatogr. A 1294 (2013) 106–116.
[33] S. Zucchi, N. Bluthgen, A. Ieronimo, The UV-absorber benzophenone-4 alters transcripts of genes involved in hormonal pathways in zebrafish (*Danio rerio*) eleuthero-embryos and adult males, Toxicol. Appl. Pharmacol 250 (2011) 137–146.
[34] S.E. Duirk, D.R. Bridenstine, D.C. Leslie, Reaction of benzophenone UV filters in the presence of aqueous chlorine: kinetics and chloroform formation, Water Res. 47 (2013) 579–587.
[35] E.D. Laurentiis, M. Minella, M. Sarakha, A. Marrese, C. Minero, G. Mailhot, M. Brigante, D. Vione, Photochemical processes involving the UV absorber benzophenone-4(2-hydroxy-4-methoxybenzophenone-5-sulphonic acid) in aqueous solution: reaction pathways and implications for surface waters, Water Res. 47 (2013) 5943–5953.
[36] M.M.P. Tsui, H.W. Leung, P.K.S. Lam, M.B. Murphy, Seasonal occurrence, removal efficiencies and preliminary risk assessment of multiple classes of organic UV filters in wastewater treatment plants, Water Res. 53 (2014) 58–67.
[37] B. Yang, G.G. Ying, Oxidation of benzophenone-3 during water treatment with ferrate (VI), Water Res. 47 (2013) 2458–2466.
[38] M.J. Frisch, G.W. Trucks, H.B. Schlegel, G.E. Scuseria, M.A. Robb, J.R. Cheeseman, J.A. Montgomery Jr., T. Vreven, K.N. Kudin, J.C. Burant, J.M. Millam, S.S. Iyengar, J. Tomasi, V. Barone, B. Mennucci, M. Cossi, G. Scalmani, N. Rega, G.A. Petersson, H. Nakatsuji, M. Hada, M. Ehara, K. Toyota, R. Fukuda, J. Hasegawa, M. Ishida, T. Nakajima, Y. Honda, O. Kitao, H. Nakai, M. Klene, X. Li, J.E. Knox, H.P. Hratchian, J.B. Cross, V. Bakken, C. Adamo, J. Jaramillo, R. Gomperts, R.E. Stratmann, O. Yazyev, A.J. Austin, R. Cammi, C. Pomelli, J.W. Ochterski, P.Y. Ayala, K. Morokuma, G.A. Voth, P. Salvador, J.J. Dannenberg, V.G. Zakrzewski, S. Dapprich, A.D. Daniels, M.C. Strain, O. Farkas, D.K. Malick, A.D. Rabuck, K. Raghavachari, J.B. Foresman, J.V. Ortiz, Q. Cui, A.G. Baboul, S. Clifford, J. Cioslowski, B.B. Stefanov, G. Liu, A. Liashenko, P. Piskorz, I. Komaromi, R.L. Martin, D.J. Fox, T. Keith, M.A. Al-Laham, C.Y. Peng, A. Nanayakkara, M. Challacombe, P.M.W. Gill, B. Johnson, W. Chen, M.W. Wong, C. Gonzalez, J.A. Pople, Gaussian 03, Revision E.01, Gaussian, Inc., Wallingford CT, 2004.
[39] K. Fukui, T. Yonezawa, T. Nagata, Molecular orbital theory of orientation in aromatic, heteroaromatic, and other conjugated molecules, J. Chem. Phys. 22 (1954) 1433–1442.
[40] K. Fukui, T. Yonezawa, H. Shingu, A molecular orbital theory of reactivity in aromatic hydrocarbons, J. Chem. Phys. 20 (1952) 722–725.
[41] X.G. Duan, H.Q. Sun, Y.X. Wang, J. Kang, S.B. Wang, N-doping-induced nonradical reaction on single-walled carbon nanotubes for catalytic phenol oxidation, ACS Catal. 5 (2015) 553–559.
[42] Y.Q. Leng, W.L. Guo, X. Shi, Y.Y. Li, L.T. Xing, Polyhydroquinone-coated Fe_3O_4 nanocatalyst for degradation of rhodamine B based on sulfate radicals, Ind. Eng. Chem. Res. 52 (2013) 13607–13612.
[43] US EPA, Toxicity Estimation Software Tool Available at: www.epa.gov/nrmrl/std/cppb/qsar/. 2012.
[44] United Nations, Globally Harmonized System of Classification and Labelling of Chemical (GHS), 4th ed., United Nations Publications, New York, 2011.